High Heat Load, High Precision Slits for the MAX Lab Multi-Pole Wiggler

Alex Deyhim, Dave Waterman, Dave Caletka

Advanced Design Consulting USA, 126 Ridge Road, P.O. Box 187, Lansing, NY 14882, USA

Abstract. Advanced Design Consulting, Inc. (ADC) has designed accurate high precision slits for applications with high heat load. The system consists of vertical and horizontal slit mechanisms, a vacuum vessel which houses them, water cooling lines with vacuum guards connected to the individual blades, stepper motors with linear encoders, limit (home position) switches and electrical connections including internal wiring for a drain current measurement system. The total slit aperture (scanable) size is 35 mm x 35 mm with maximum aperture of 50 mm x 50 mm. Each of the four blades are individually controlled and motorized. In this paper, a summary of the design and Finite Element Analysis of the system are presented.

Summary:

A thermal / mechanical analysis has been performed on the water cooled secondary slits for Max Lab. Results show that, for a nominal power density of 30 W/mm^2, applied evenly over an area of 70 mm^2 between upper and lower slit edges, the deformation of the upper and lower slit edges is typically less than 15μ. The slit edge deformation is essentially constant for water flow rates ranging from 0.5 gpm to 3.0 gpm. There is also a translation and rotation of the slit edges, that will affect the true position of and anticipated gap between the two opposing blade edges. This deviation from true position of the blade edges is due to the temperature distribution and subsequent thermal expansion within the copper blade mounts, tungsten blades and stainless steel cooling / support tubes, resulting from the incident radiation. For a minimal water flow rate of 0.5 gpm, the magnitude of the blade edge translation is -19.8μ (upper blade) and 101.3μ (lower blade). The consequence of these translations tends to reduce the expected blade gap. Blade rotation is calculated to be 736 μ-rad (upper blade) and 287 μ-rad (lower blade). The combination of translation, rotation, and deformation results in an 82.4 - 106μ reduction in the anticipated gap between blade edges at a 0.5 gpm cooling water flow rate. At a flow rate of 3.0 gpm, the reduction in anticipated gap is between 99 - 113μ, with a blade edge translation of -38.8μ (upper blade) and 81.0μ (lower blade).

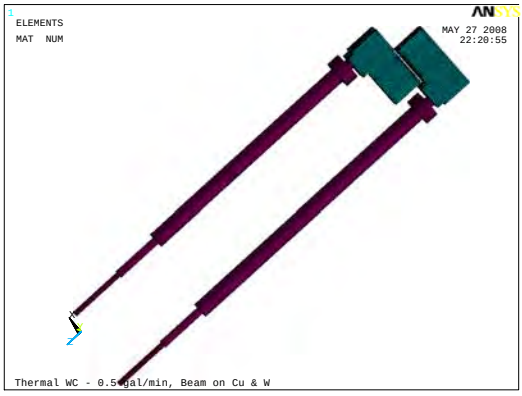

(a)

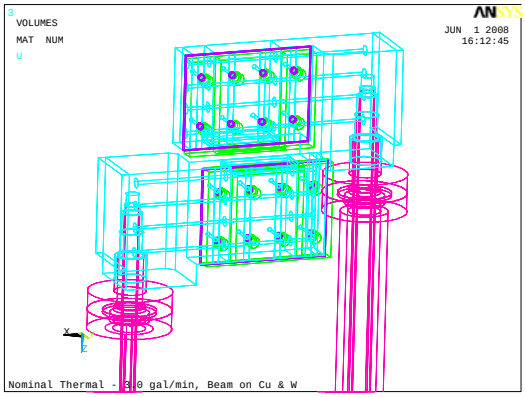

(b)

Figure 1 – Water cooled slit finite element model / geometry

Although not included in this report, one of the major design variables influencing assembly temperature, other than water flow rate, that was investigated during the course of this analysis, was the amount of overhang of the tungsten blade with respect to the copper cooling block. The lower this overhang is, the less power that is incident on the tungsten and subsequently, the lower the blade temperature. A higher percentage of the power is absorbed in the copper cooling block, which is much more efficiently removed by the flow of cooling water. Assuming the flow can be controlled, i.e., no cavitation or stagnation points, the highest possible flow rate should be used in order to cool the copper block(s). As an example, the current design analyzed includes an overhang of 0.5mm for which a peak blade temperature of 1135°C is calculated for nominal power levels of 1050W per blade. Compare this to 1808°C when the overhang is 1mm and the input power to the blade is doubled.

As previously implemented, the greatest contributor to this gap reduction and deviation from true position can potentially be controlled via strategic temperature measurement on the copper blade holders and / or stainless steel cooling / support tubes and

subsequent compensation. Note that up to 1/3 of the total vertical translation is attributable to expansion of the stainless support tubes and that zero deflection is assumed at the control motors.

Assumptions (Cooling):

Cooling of the slits is accomplished via conduction through the various components and interfaces of the assembly along with convection to the water running through the annular tubes within the stainless steel supports and cooling channels within the copper blade holding blocks (see Figure 1b). As this is a vacuum application, no external convection was assumed in the thermal simulations. The motor ends of the stainless steel support tubes were held constant @ 30°C. Radiation was also included in the thermal simulations in light of the relatively high power being evaluated. The pertinent parameters related to the cooling scheme are the thermal properties of the materials involved, the thermal contact resistance at various bolted interfaces, the convective heat transfer properties afforded by the water flow and the emissivity's of various surfaces. Emissivity was conservatively assumed to be 0.4 for all surfaces. Other thermal properties and contact resistance values are calculated and listed in the attachment in Appendix A.

In order to calculate the convective heat transfer coefficient(s) associated with the water flow in the annular cooling tube and copper block flow channels, several flow conditions were evaluated so as to insure that the flow would be turbulent in order to maximize heat transfer. The water properties, flow conditions and convection coefficients are also listed in the attachment in Appendix A[1]. Note that for Reynolds numbers above ~3000, the following convection correlation for transition and turbulent flow is used [2]:

$$Nu_D = \frac{(f/8)(\mathrm{Re}_D - 1000)\,\mathrm{Pr}}{1 + 12.7(f/8)^{1/2}(\mathrm{Pr}^{2/3} - 1)} \quad [1]$$

where: $f = (0.790 \ln \mathrm{Re}_D - 1.64)^{-2}$. [2]

The convection coefficient is defined as $h = kNu_D / D_H$. [3]

Re_D and Pr are defined in the attachment. These correlations have been shown to be valid for $0.5 < \mathrm{Pr} < 2000$ and $3000 < \mathrm{Re}_D < 5\text{x}10^6$.

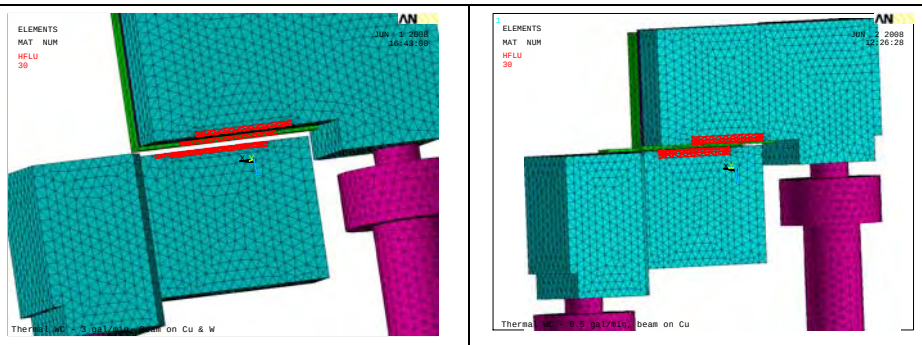

(a) (b)

Figure 2 – Finite element model depicting areas of applied heat flux (30 Watts/mm^2); (a) – Nominal condition, 1050 watts per blade centered on blade overlap – 28mm x 1.25mm, (b) – worst case condition, 2100 watts per blade applied totally on the copper cooling blocks.

Model Assumptions:

ANSYS 8.1 ® was used for the steady state thermal and mechanical simulations presented herein. Approx. 150,000 - quadratic tetrahedral, pyramid, and hexahedral elements were employed to model the water cooled slits assembly. Thermal contact resistance and mechanical contact at the bolted interfaces (tungsten blade / macor insulator and macor insulator / copper cooling block) were simulated with surface-to-surface contact elements. Calculations for thermal contact resistance were based on an average contact pressure of 176 psi due to tightening of the eight tantalum bolts to a torque of 0.18 – 0.22 Nm (see attachment). This torque value is based on the yield strength of RO5200 / RO5400 tantalum which is similar to a class 4.8 metric steel fastener. The tantalum bolts were represented by conduction link elements in the thermal analysis and 3D beam elements in the mechanical simulations. Constraint equations were utilized in connecting the beam elements to the solid elements of the tungsten blades and copper blocks. All relevant material properties are listed in the attachment.

As this is a vacuum application, no free convection was specified for external surfaces. Radiation, however, was included resulting in a non-linear solution. Figure 2 shows the finite element mesh and the areas on the slit blades and cooling blocks where the heat flux was applied. Although not shown in the figure, convective heat transfer coefficients (see attachment) were specified on the inner wall(s) of the annular cooling tube along with the cooling channels within the copper cooling blocks. Note in Figure 1 (b) that the input of the cooling tubes to the copper block cooling channels is different between the upper and lower slits with respect to the proximity to the area of incident radiation. In all simulations, the applied heat flux was 30 W/mm^2. Two thermal loading conditions were considered, nominal and worst case. Nominal conditions are assumed to be normal operating conditions, i.e., centered beam, 2100 W at 30 W/mm^2 divided evenly between the two blades assemblies. It is under these conditions that blade deformation is considered critical. Under worst case conditions, the assumption is that the beam (2100 W, 30 W/mm^2) is incident on only one of the blade assemblies. The total power incident during the worst case simulations was actually 4200W as each of the blade assemblies, which are essentially thermally independent with the exception of radiation, were subject to the full 2100W. Further, worst case conditions were evaluated such that the beam was either incident on only the copper cooling block(s), or a combination of the (0.5mm x 28mm) overlapped tungsten blade and (2.0mm x 28mm) of the copper cooling block. Each loading condition was evaluated at two cooling water flow rates; 0.5 gpm and 3.0 gpm.

Once the thermal simulations were run, the resulting temperature distributions were applied as thermal loads to the mechanical version of the model. Full restraint was applied to each blade assembly at the "motor end" of the stainless steel support tube(s). The effect of bolt tightening was included in the first load step of each mechanical simulation. An initial strain corresponding to 70% of the proof load for a class 4.8 M2 fastener was applied to the 3D beam elements representing the tantalum bolts. The increase in bolt tension subsequent to application of thermal loads was typically only 5-10% of proof load.

Results / Discussion:

Thermal Results:

Table 1 and Figures 3 through 8 summarize the thermal results of the various simulations. Temperature ranges observed in each part of the slit assembly are listed in Table 1 for both the upper and lower blade assemblies. The upper blade assembly invariably exhibits higher maximum temperatures than the lower blade assembly does due to the relative position of the annular cooling tube inlet with respect to the area of applied heat flux. The results in Table 1 indicate that as long as the flow is turbulent (< 0.45 gpm, see attachment), the tungsten blade temperatures do not significantly vary (<25°C) over the range of flow rates evaluated. This is primarily due to the conservative nature of the thermal contact conductance calculated for the various interfaces. As less and less of the tungsten blade is subject to incident radiation, i.e., lower tungsten overhang, the effectiveness of increased water flow rates increases while the detrimental effect of interfacial contact conductance decreases with respect to heat removal from the assembly.

Nominal Heat Load		Cu Temp. (°C)		Macor Temp. (°C)		Blade Temp. (°C)		Cooling Tube Wall Temp. (°C)		See Figure #
Water Flow Rate	Beam Incidence	Min	Max	Min	Max	Min	Max	Min	Max	
0.5 gpm	Cu & Tungsten	**38.3**	**197.7**	**116.6**	**538.7**	**750.7**	**1135**	**30.0**	**51.1**	3
3.0 gpm		**30.5**	**154.9**	**104.7**	**515.1**	**737.6**	**1123**	**30.0**	**42.4**	4
Worst Case Heat Load		Cu Temp. (°C)		Macor Temp. (°C)		Blade Temp. (°C)		Cooling Tube Wall Temp. (°C)		See Figure #
Water Flow Rate	Beam Incidence	Min	Max	Min	Max	Min	Max	Min	Max	
0.5 gpm	Cu Only	**42.6**	**461.3**	**53.8**	**168.5**	**84.8**	**96.9**	**30.0**	**53.2**	5
3.0 gpm		**30.5**	**353.9**	**32.6**	**79.4**	**41.3**	**45.1**	**30.0**	**33.9**	6
0.5 gpm	Cu & Tungsten	**42.9**	**385.7**	**123.9**	**583.1**	**764.9**	**1150**	**30.0**	**57.6**	7
3.0 gpm		**30.6**	**291.6**	**105.1**	**528.9**	**740.2**	**1126**	**30.0**	**43.0**	8

Table 1 – Thermal Results – Calculated temperature ranges

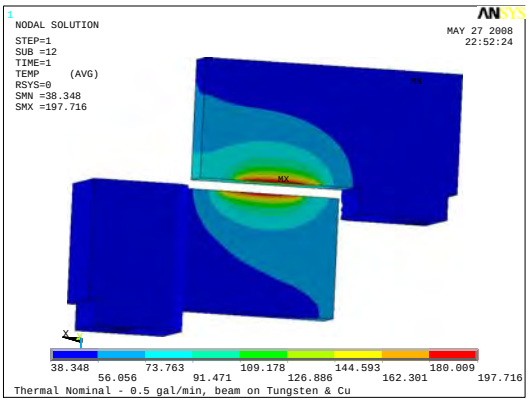

(a)

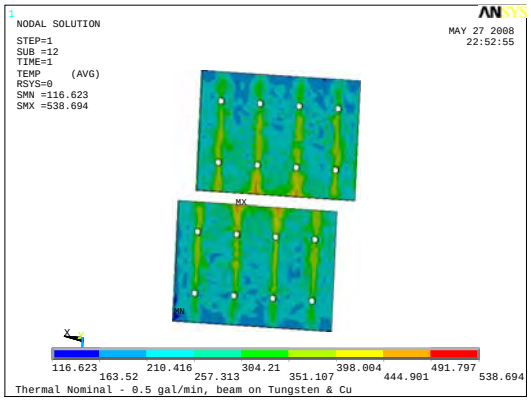

(b)

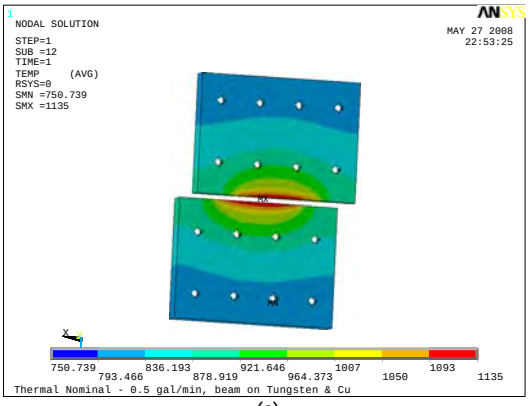

(c)

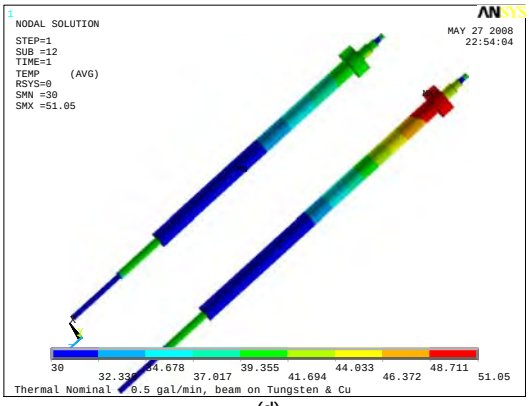

(d)

Figure 3 – Temperature Distribution, Nominal heat load, 0.5 gpm; (a) – Copper blocks, (b) – Macor Insulators, (c) – Tungsten blades, (d) – Cooling tube walls

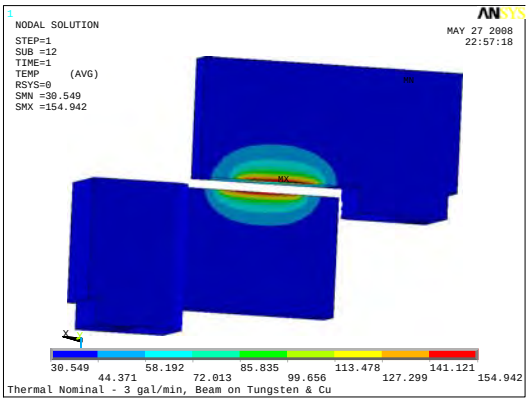

(a)

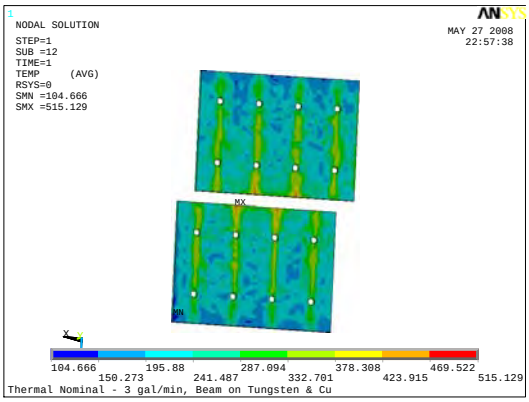

(b)

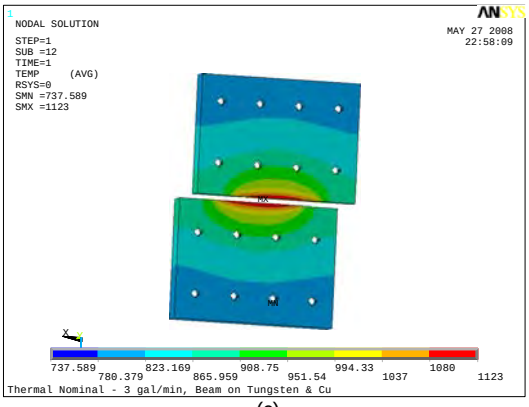

(c)

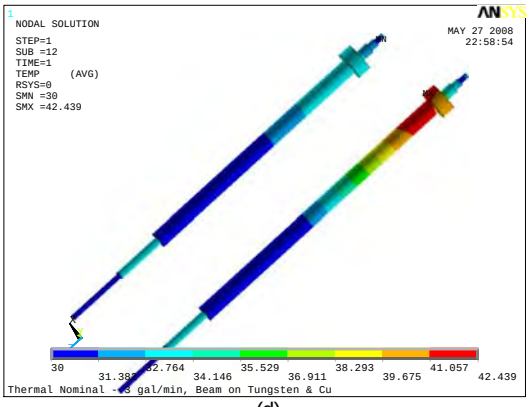

(d)

Figure 4 – Temperature Distribution, Nominal heat load, 3.0 gpm; (a) – Copper blocks, (b) – Macor Insulators, (c) – Tungsten blades, (d) – Cooling tube walls

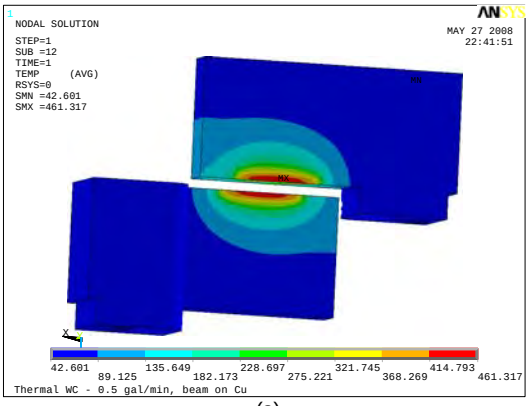

(a)

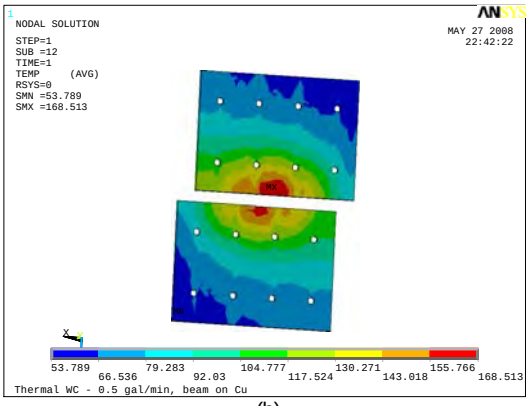

(b)

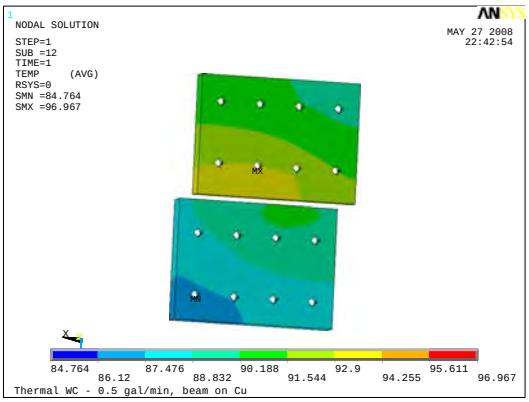

(c)

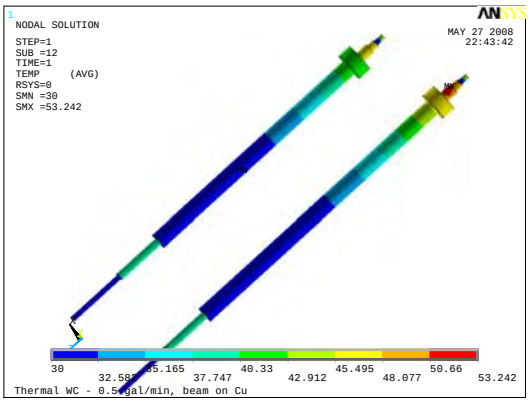

(d)

Figure 5 – Temperature Distribution, Worst Case heat load, 0.5 gpm, Beam incidence Cu only; (a) – Copper blocks, (b) – Macor Insulators, (c) – Tungsten blades, (d) – Cooling tube walls

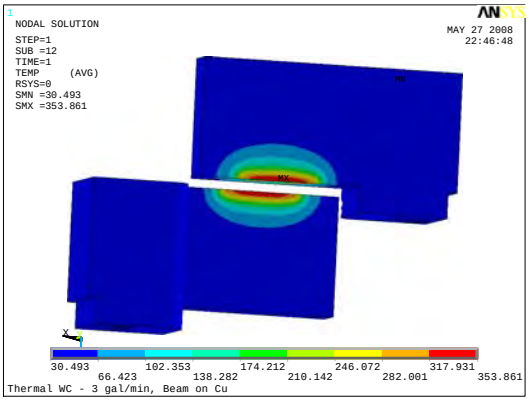

(a)

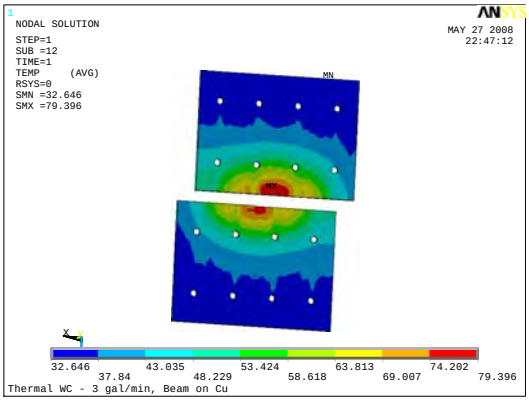

(b)

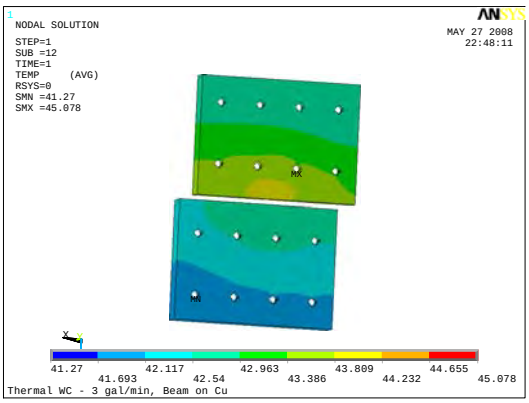

(c)

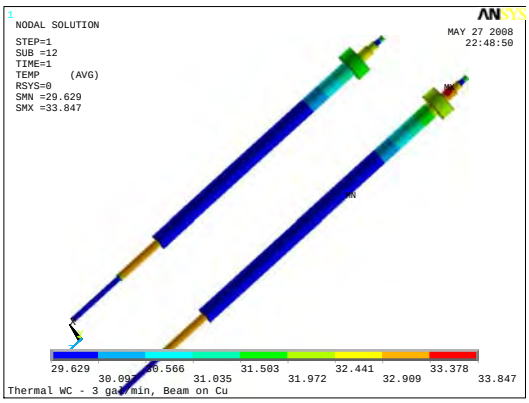

(d)

Figure 6 – Temperature Distribution, Worst Case heat load, 3.0 gpm, Beam incidence Cu only; (a) – Copper blocks, (b) – Macor Insulators, (c) – Tungsten blades, (d) – Cooling tube walls

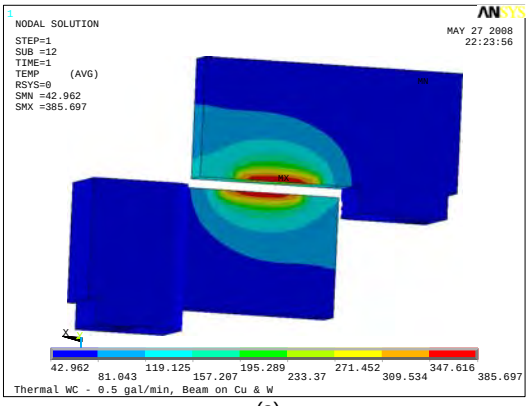

(a)

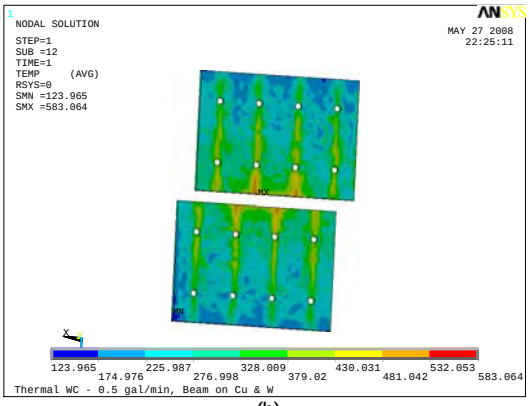

(b)

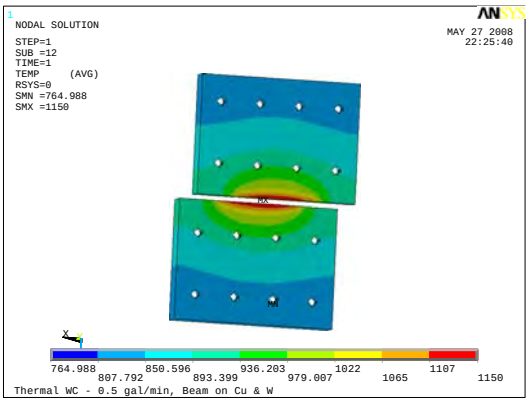

(c)

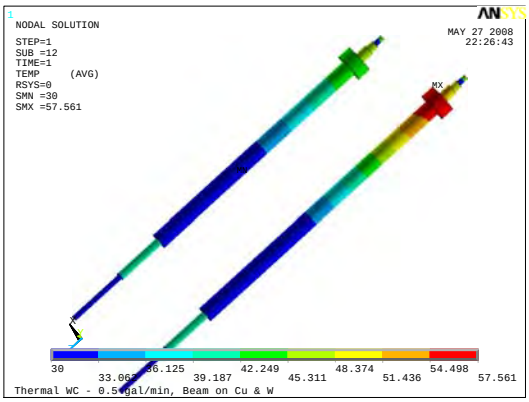

(d)

Figure 7 – Temperature Distribution, Worst Case heat load, 0.5 gpm, Beam incidence Cu & W blades; (a) – Copper blocks, (b) – Macor Insulators, (c) – Tungsten blades, (d) – Cooling tube walls

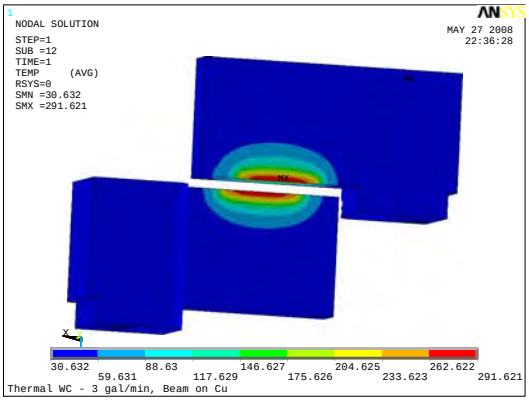

(a)

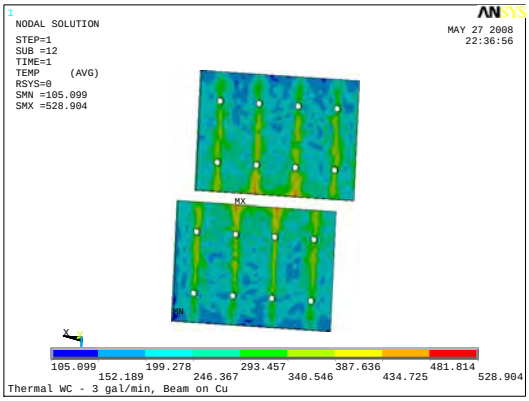

(b)

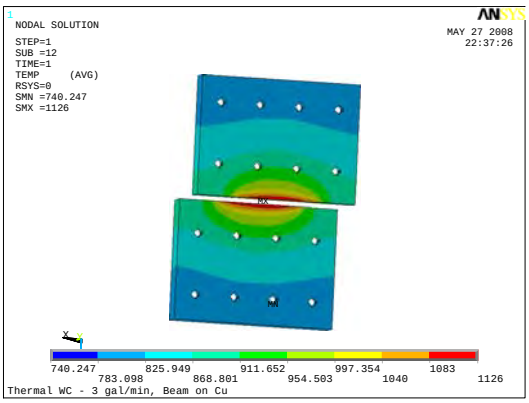

(c)

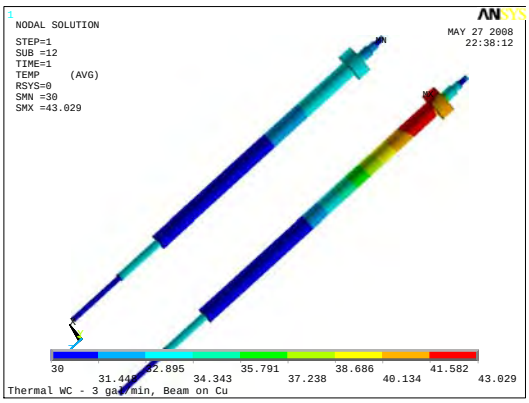

(d)

Figure 8 – Temperature Distribution, Worst Case heat load, 3.0 gpm, Beam incidence Cu & W blades; (a) – Copper blocks, (b) – Macor Insulators, (c) – Tungsten blades, (d) – Cooling tube walls

Mechanical Results:

Table 2 and Figures 10 through 15 summarize the mechanical results of the various simulations. The coordinate system utilized is shown in Figure 9 along with the location on the blade edges where vertical blade translation (Uz) and rotation listed in Table 2 are referenced from. Figures 10 through 15 show the displacements (Ux, Uy and Uz) of the slit assemblies along with a plot of the vertical (Uz) displacement / deformation along the opposing blade edges from left to right as viewed in Figure 9. Note however that positive vertical (Z) displacements listed in Table 2 and plotted in the graphs of Figures 10 – 15 are upward, contrary to the contour plots in Figures 10 – 15 (c) and the coordinate system depicted in Figure 9.

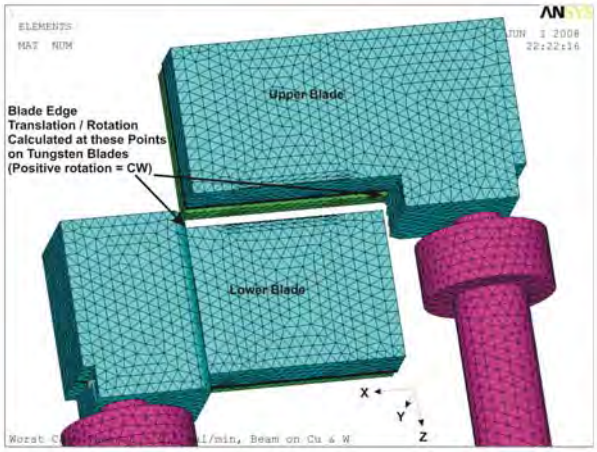

Figure 9 – Coordinate definition

As can be seen in Table 2, under nominal heat loading, overall translation of the opposing blade edges varies by about 20μ over a flow range of 0.5 – 3.0 gpm. Blade edge deformation is essentially unaffected by the evaluated cooling water flow rates.

The results presented in the "blade edge deformation vs distance along blade edge" plots in Figures 10 and 11 (nominal heat load cases) are based on initial opposing blade edge positions of 0μ and 0μ respectively for the lower and upper blades. The plots therefore show the final position / deformation of the blade edge(s) upon application of thermal loads. Typically the blade edges move up vertically (by unequal amounts) and the resulting blade overlap is more than the 0μ anticipated. The change in true position of the blade edges is a result of the thermal expansion of both the copper blocks, the stainless steel cooling / support tubes and the tungsten blades that are effectively expanding about the center of the tantalum bolt pattern. Therefore, for the lower blade assembly, the expansion of the copper, tungsten and stainless steel tend to be additive whereas for the upper blade assembly, the tungsten blade expansion is in effect subtracted from that of the copper and stainless steel.

The plots in Figures 12 through 15, which are included for reference purposes as they do not apply to normal operating conditions, are also based on initial opposing blade edge positions of 0μ and 0μ respectively for the lower and upper blades. These plots show the deformation(s) resulting from the worst case conditions where all 2100W is incident on either the upper of lower blade assembly.

Global bending stress within the Macor insulator(s) did not exceed 75 Mpa for any of the simulations and was typically lower than 50 MPa under nominal conditions. Flexural strength of the Macor is quoted to be 94 Mpa by Corning. Evaluation of localized stresses within the Macor insulator(s) in the vicinity of the tantalum bolts would require additional computational effort which was beyond the scope of the present analysis.

Nominal Heat Load		Vertical Translation (μ)		Rotation (μ-rad)		Tungsten Blade Edge Deformation (μ)		See Figure #
Water Flow Rate	Beam Incidence	Upper	Lower	Upper	Lower	Upper	Lower	
0.5 gpm	Cu & Tungsten	**-19.79**	**101.28**	**735.8**	**286.9**	**13.83**	**14.54**	10
3.0 gpm		**-38.75**	**81.04**	**392.7**	**135.1**	**13.69**	**14.43**	11
Worst Case Heat Load								
		Vertical Translation (μ)		Rotation (μ-rad)		Tungsten Blade Edge Deformation (μ)		See Figure #
Water Flow Rate	Beam Incidence	Upper	Lower	Upper	Lower	Upper	Lower	
0.5 gpm	Cu	**21.23**	**49.72**	**1750**	**1250**	**0**	**0**	12
3.0 gpm		**-6.27**	**11.99**	**796.4**	**617.4**	**0**	**0**	13
0.5 gpm	Cu & Tungsten	**-11.66**	**120.34**	**1560**	**961.1**	**14.27**	**14.94**	14
3.0 gpm		**-41.62**	**85.93**	**759.8**	**473.3**	**13.91**	**14.63**	15

Table 2 – Mechanical Results – Blade edge displacement / deformation

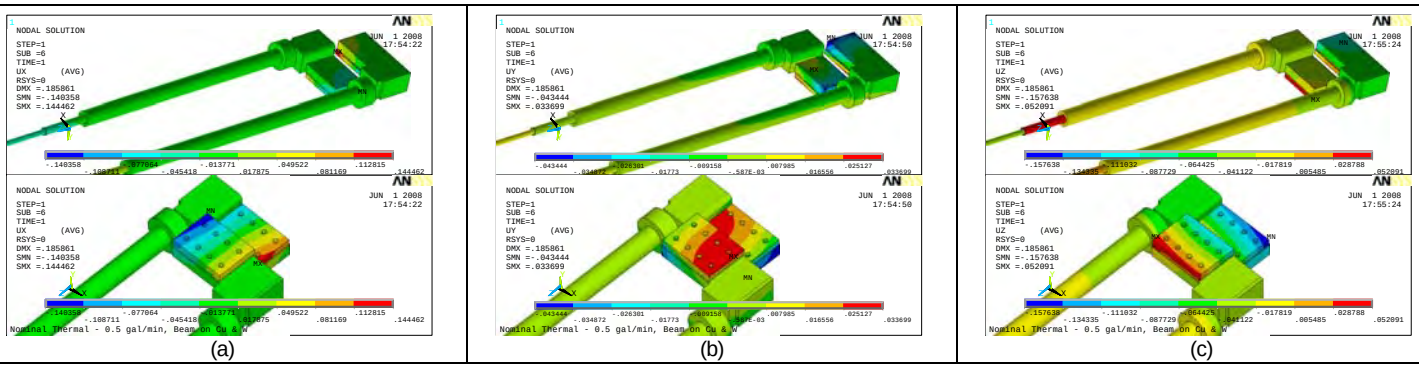

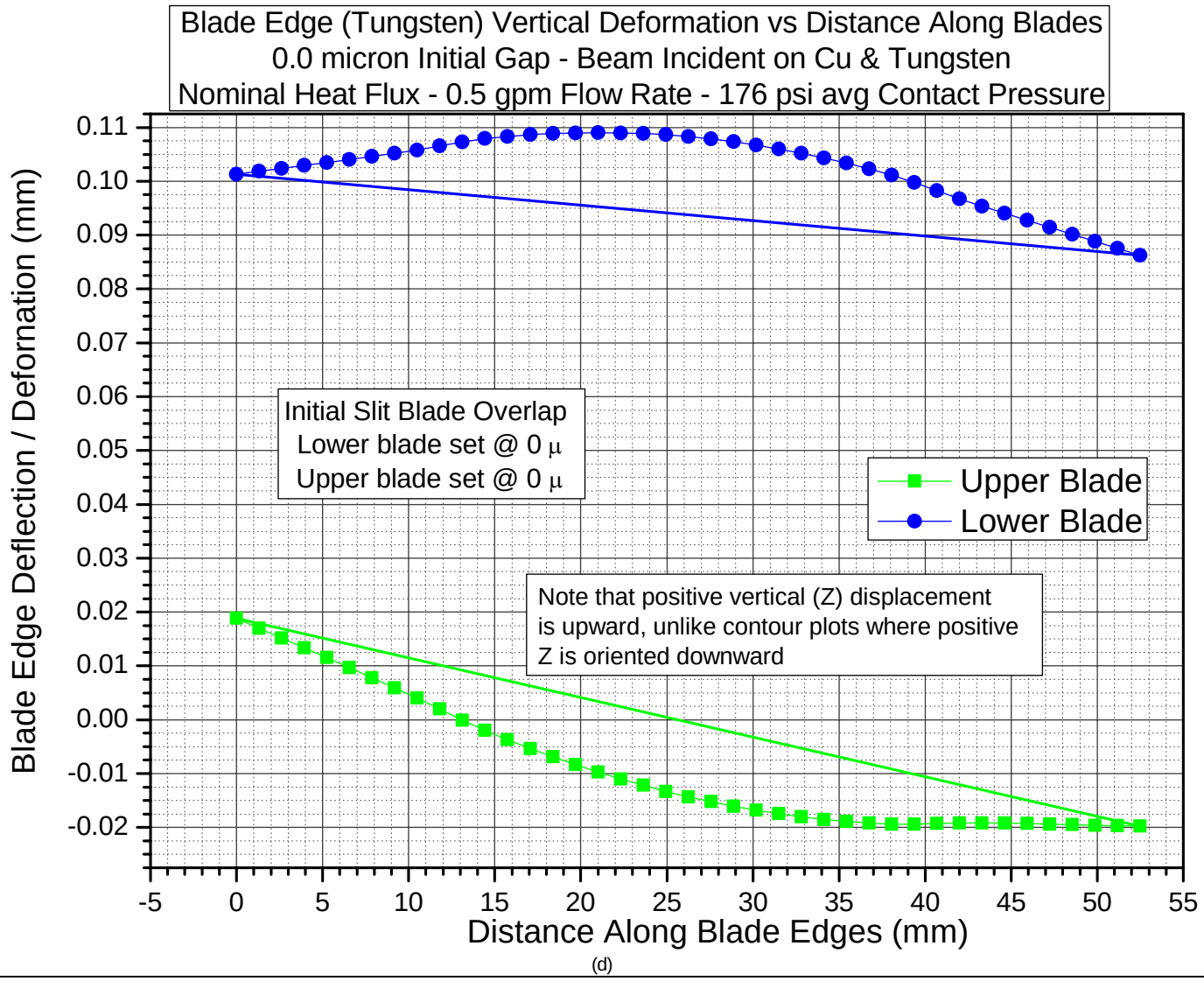

(d)

Figure 10 – Slit assembly deformation – Nominal heat load, 0.5 gpm, Beam Incident on Cu & W Blades; (a) – Ux, (b) – Uy, (c) – Uz, (d) Blade edge deformation

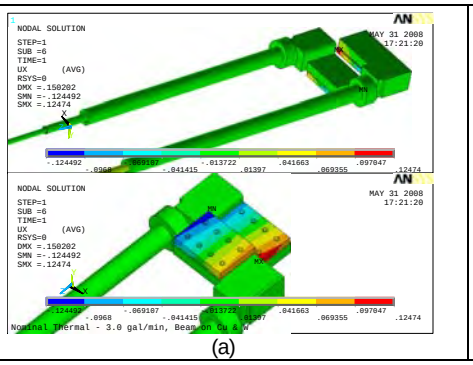

(a)

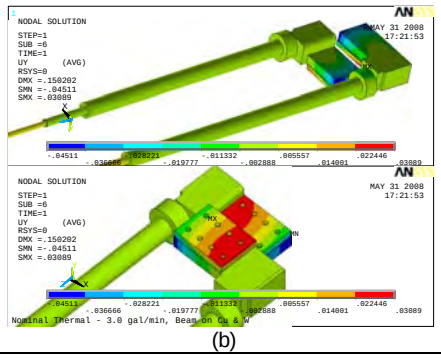

(b)

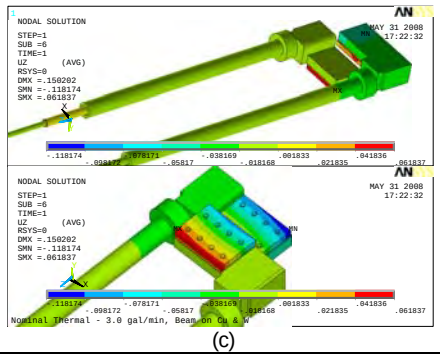

(c)

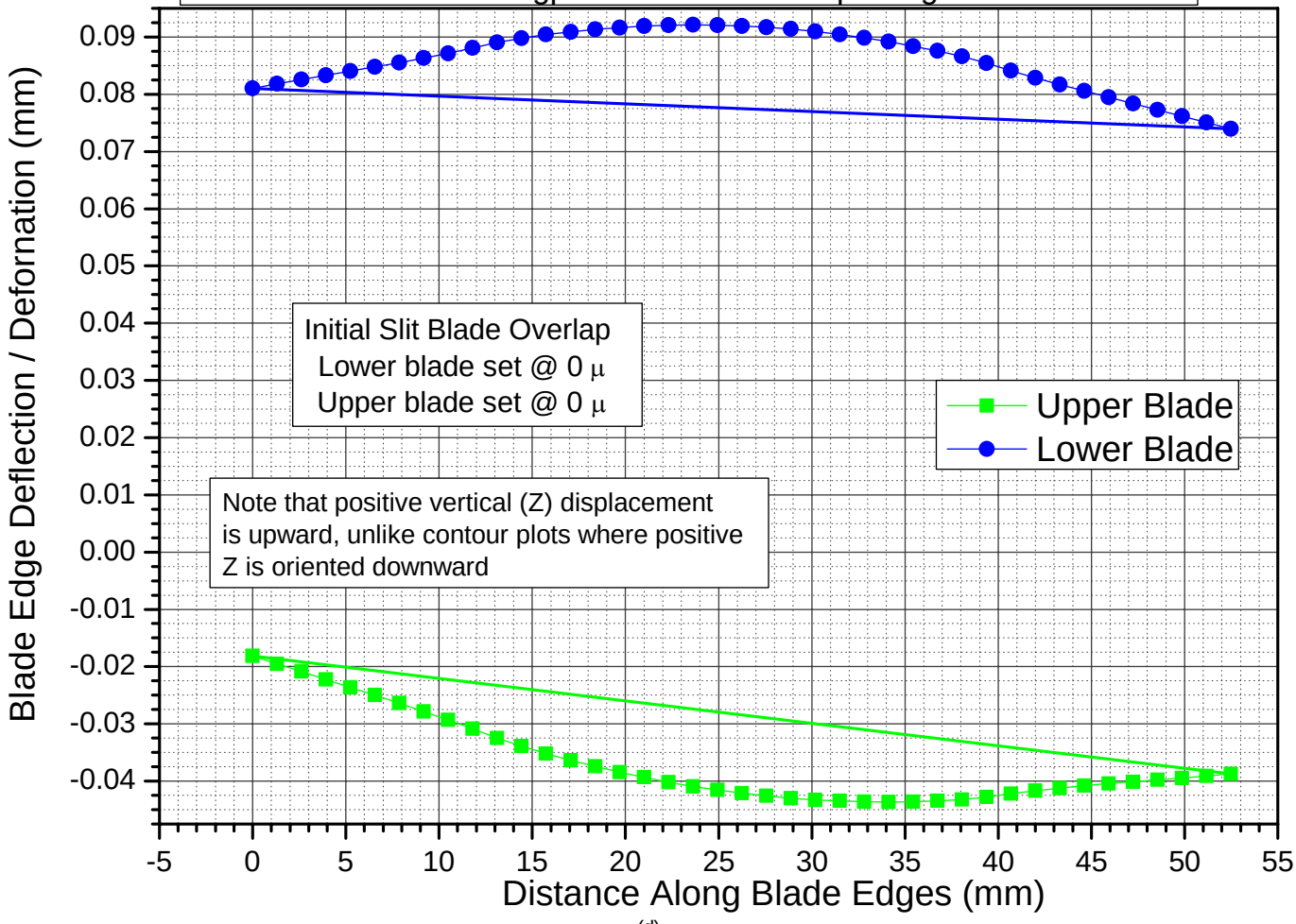

(d)

Figure 11 – Slit assembly deformation – Nominal heat load, 3.0 gpm, Beam Incident on Cu & W Blades (a) – Ux, (b) – Uy, (c) – Uz, (d) Blade edge deformation

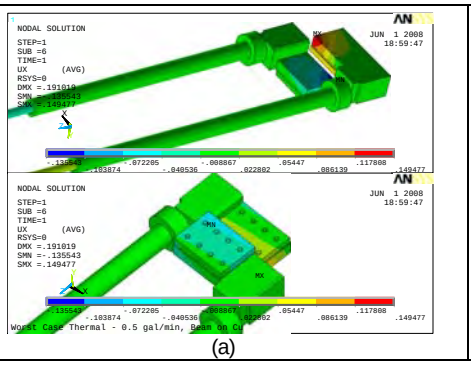

(a)

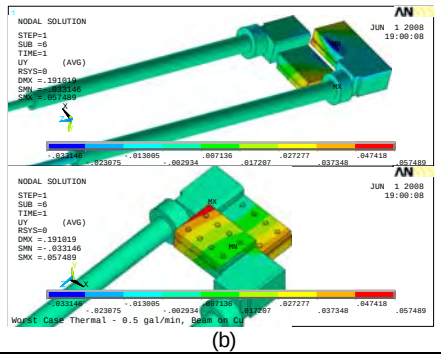

(b)

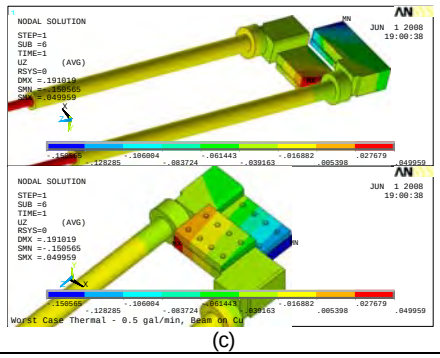

(c)

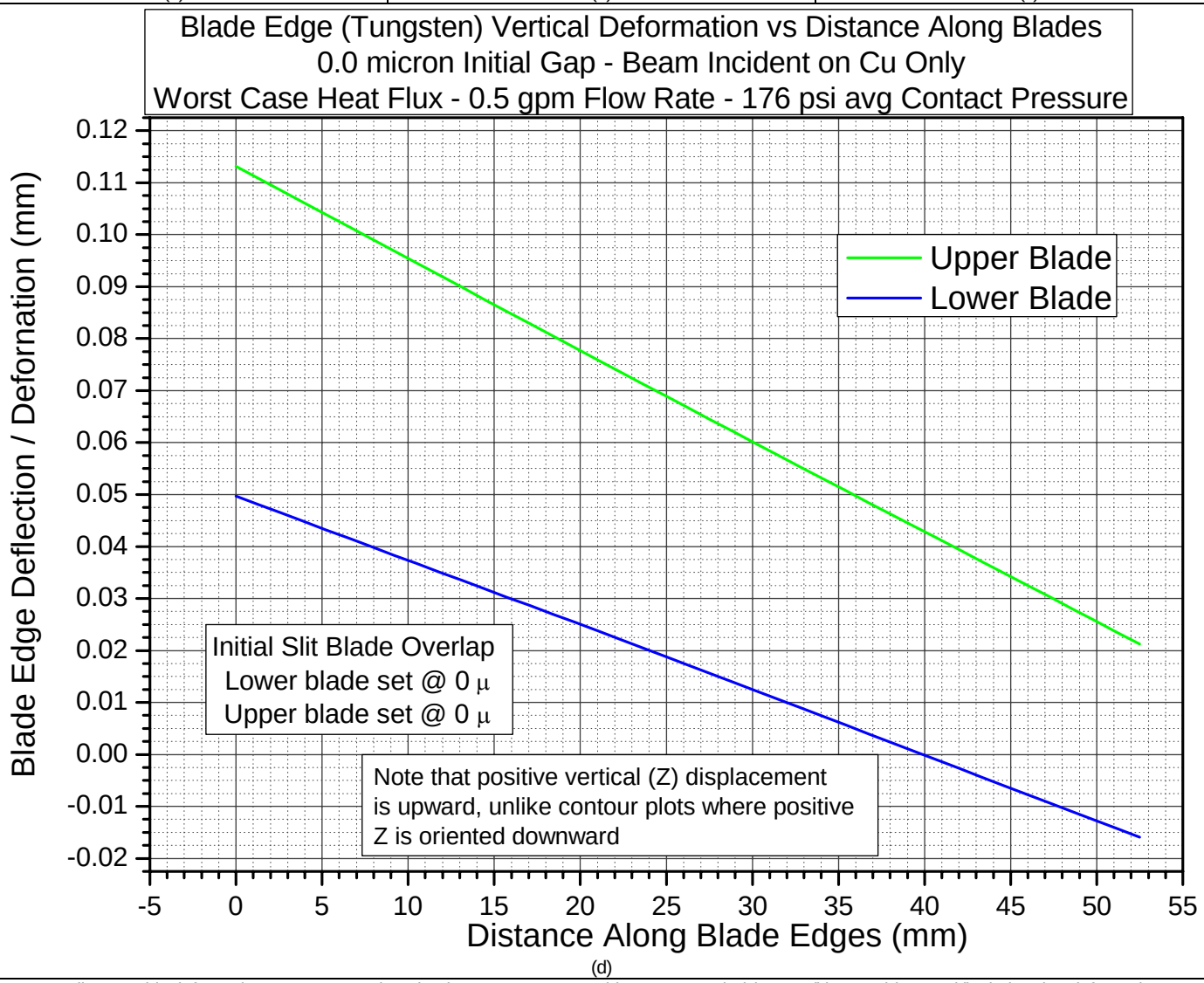

(d)

Figure 12 – Slit assembly deformation – Worst Case heat load, 0.5 gpm, Beam Incident on Cu Only (a) – Ux, (b) – Uy, (c) – Uz, (d) Blade edge deformation

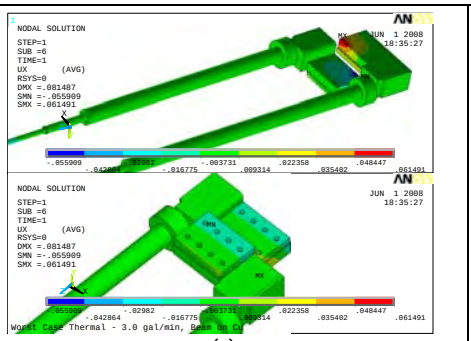

(a)

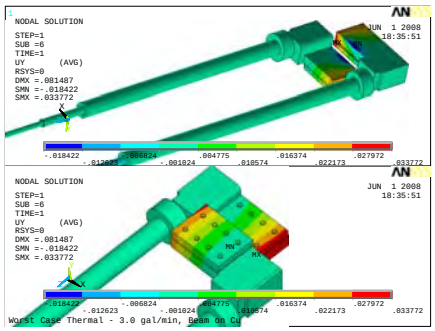

(b)

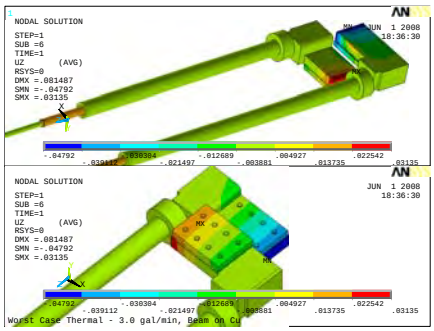

(c)

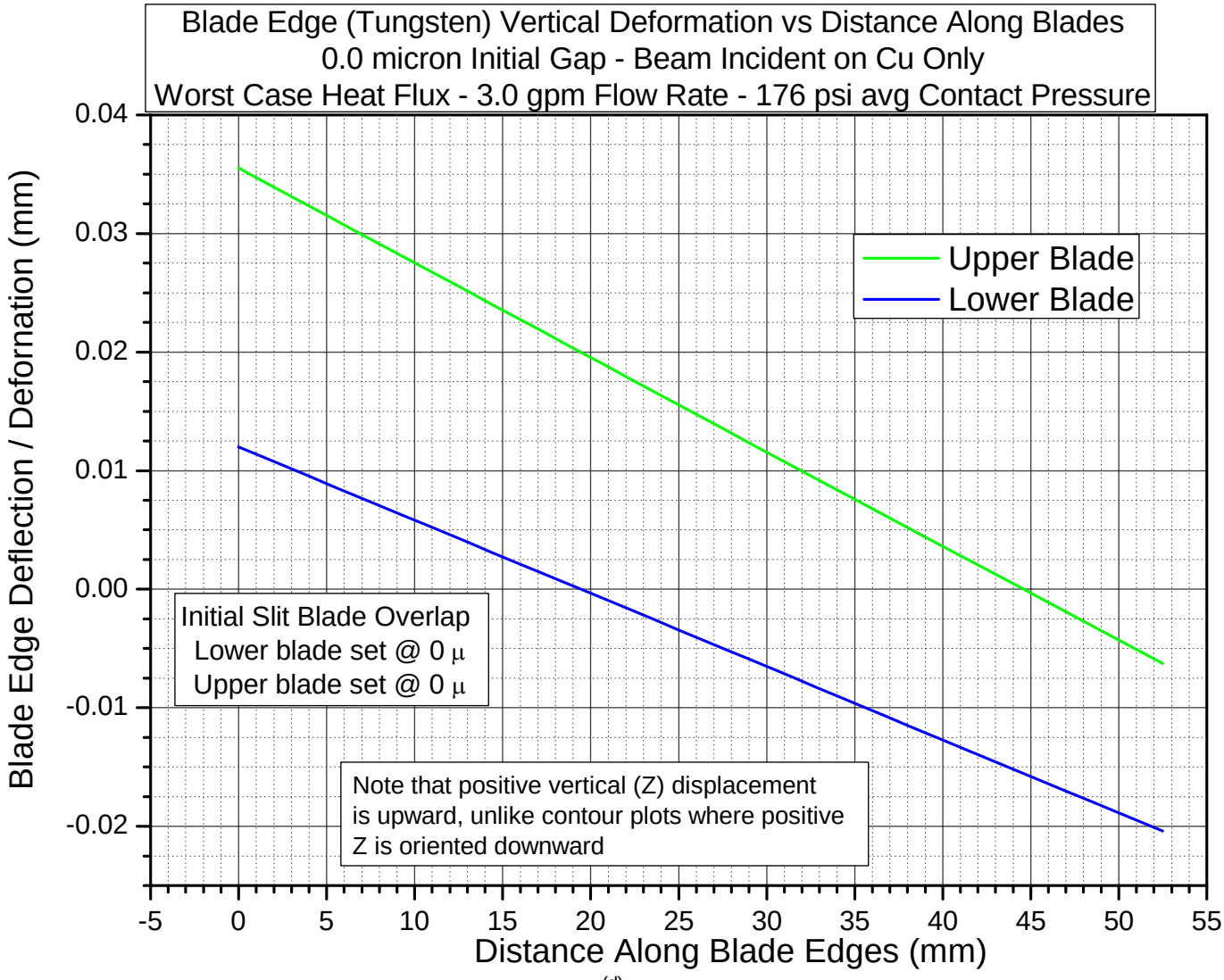

(d)

Figure 13 – Slit assembly deformation – Worst Case heat load, 3.0 gpm, Beam Incident on Cu Only (a) – Ux, (b) – Uy, (c) – Uz, (d) Blade edge deformation

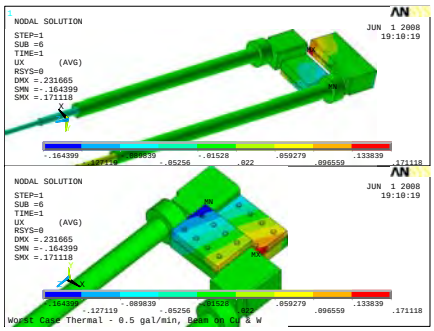

(a)

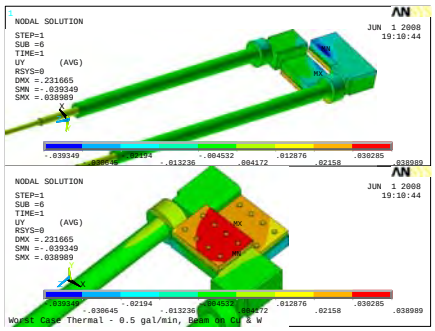

(b)

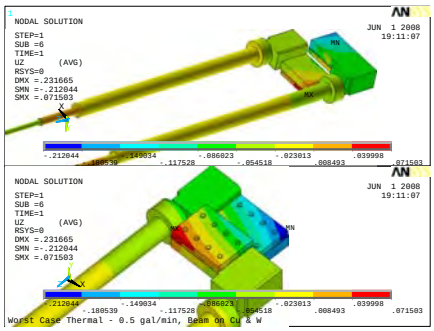

(c)

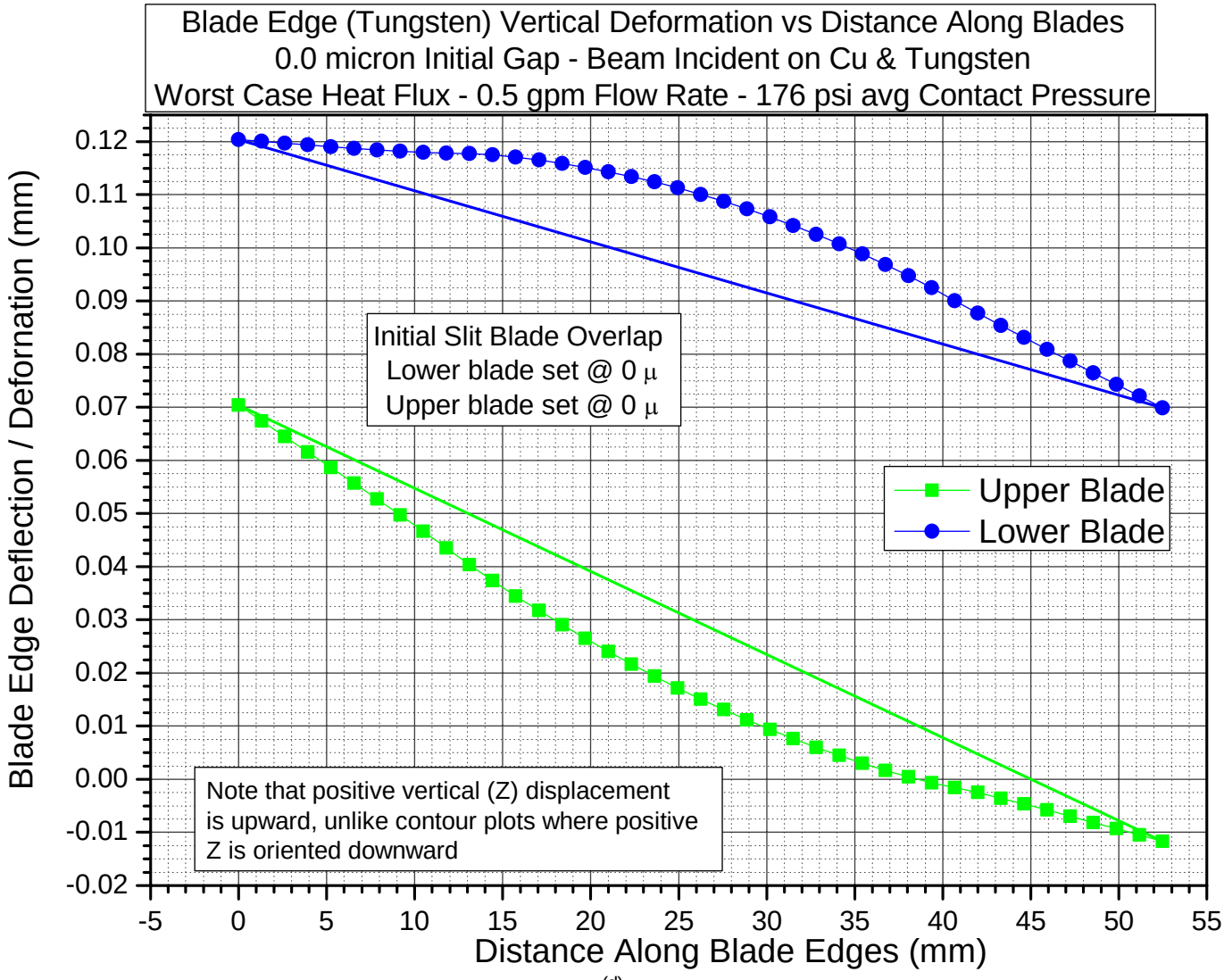

(d)

Figure 14 – Slit assembly deformation – Worst Case heat load, 0.5 gpm, Beam Incident on Cu & W Blades (a) – Ux, (b) – Uy, (c) – Uz, (d) Blade edge deformation

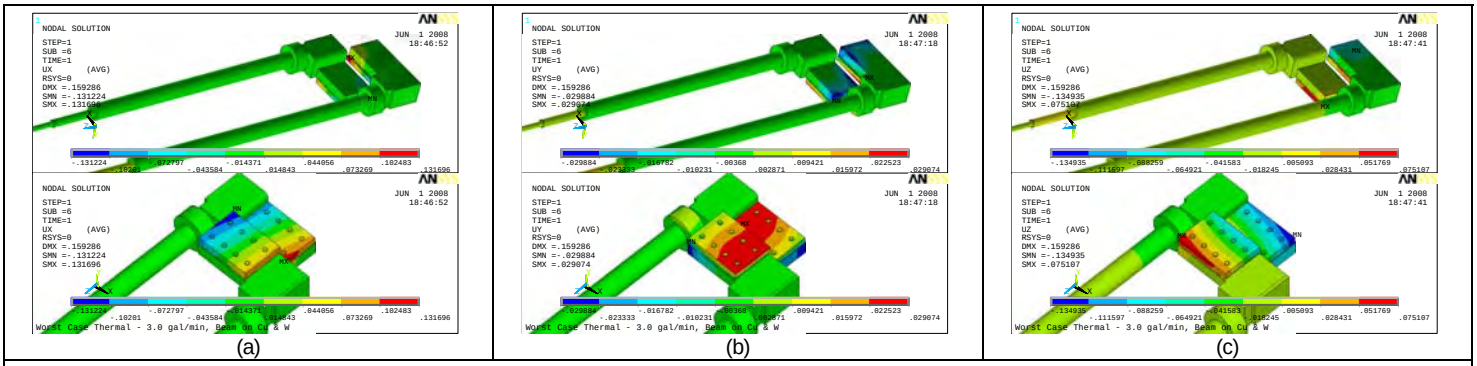

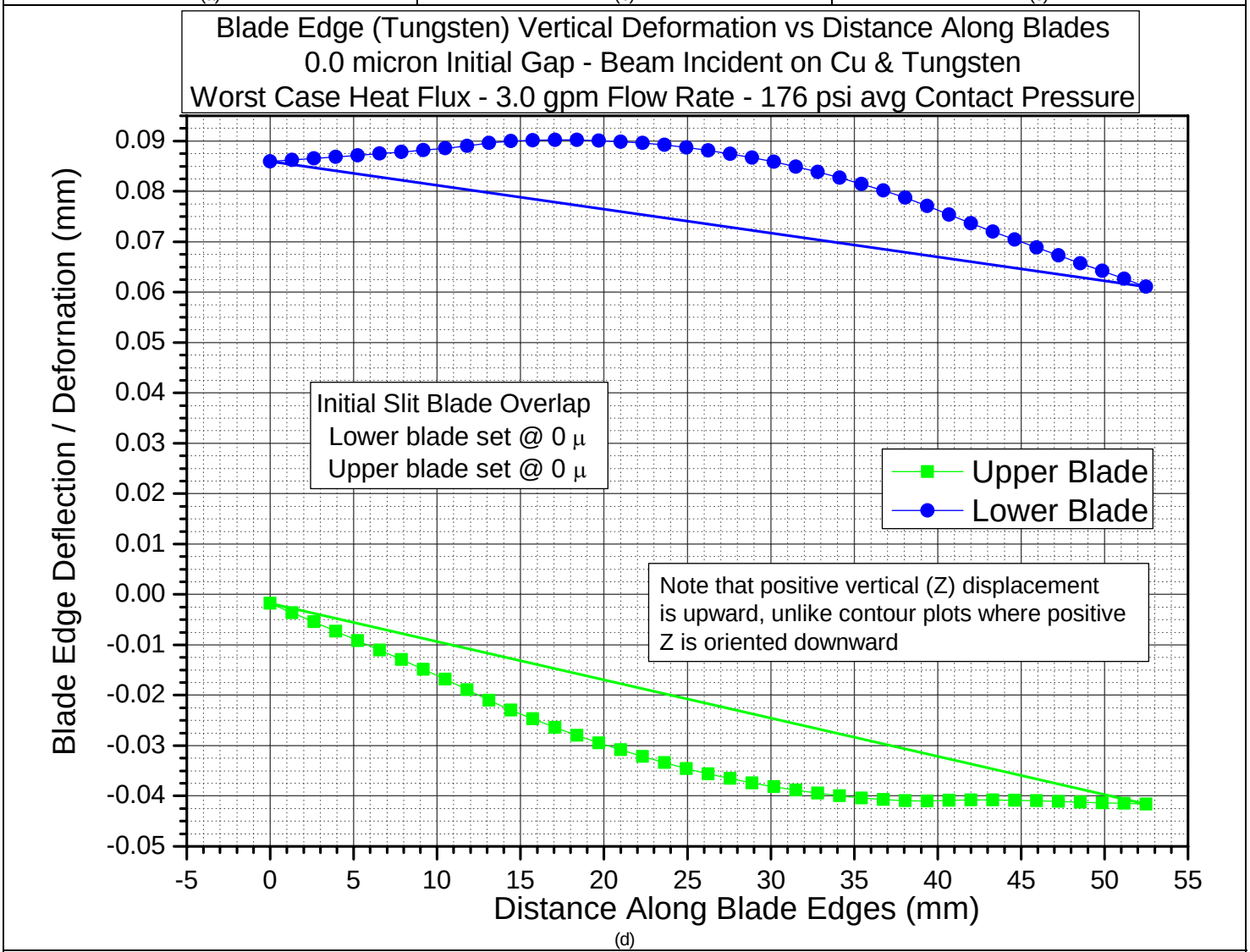

(d)

Figure 15 – Slit assembly deformation – Worst Case heat load, 0.5 gpm, Beam Incident on Cu & W Blades (a) – Ux, (b) – Uy, (c) – Uz, (d) Blade edge deformation

Conclusions:

Results from the present thermal / mechanical simulations show that, for a nominal power density of 30 W/mm^2, applied evenly over an area of 70 mm^2 between upper and lower slit edges, the deformation of the upper and lower slit edges is typically less than 15μ. The slit edge deformation is essentially constant for water flow rates ranging from 0.5 gpm to 3.0 gpm. There is also a translation (-40 – 100μ) and rotation of the slit edges (135 – 736 μ-rad) that will affect the true position of, and anticipated gap between, the two opposing blade edges. This deviation from true position of the blade edges is due to the temperature distribution and subsequent thermal expansion within the copper blade mounts, tungsten blades and stainless steel cooling /

support tubes resulting from the incident radiation. The overall blade edge translation varies less than 20μ over the range of cooling flow rates considered.
Although not included in this report, one of the major design variables influencing assembly temperature, other than water flow rate, that was investigated during the course of this analysis, was the amount of overhang of the tungsten blade with respect to the copper cooling block. The lower this overhang is, the less power that is incident on the tungsten and subsequently, the lower the blade temperature. A higher percentage of the power is absorbed in the copper cooling block, which is much more efficiently removed by the flow of cooling water. Assuming the flow can be controlled, i.e., no cavitation or stagnation points, the highest possible flow rate should be used in order to cool the copper block(s).
As previously implemented, the greatest contributor to this gap reduction and deviation from true position can potentially be controlled via strategic temperature measurement on the copper blade holders and / or stainless steel cooling / support tubes and subsequent compensation.

Appendix A:

H2O Slits Properties.xls

[1] Incropera and DeWitt, Fundamentals of Heat and Mass Transfer, Wiley, New York, 1990
[2] Petukhov and Hartnett, Advances in Heat Transfer, vol. 6, Academic Press, NY, 1970